Journal of Alzheimer's Disease 21 (2010) 119–132
DOI 10.3233/JAD-2010-100066
IOS Press

Calretinin Interneurons are Early Targets of Extracellular Amyloid-β Pathology in PS1/AβPP Alzheimer Mice Hippocampus

David Baglietto-Vargas[a,b,1], Ines Moreno-Gonzalez[a,b,1], Raquel Sanchez-Varo[a,b,1], Sebastian Jimenez[b,c,d], Laura Trujillo-Estrada[a,b], Elisabeth Sanchez-Mejias[a,b], Manuel Torres[b,c,d], Manuel Romero-Acebal[b,e], Diego Ruano[b,c,d], Marisa Vizuete[b,c,d], Javier Vitorica[b,c,d] and Antonia Gutierrez[a,b,*]

[a]*Dpto. Biología Celular, Genética y Fisiología, Facultad de Ciencias, Universidad de Málaga, Spain*
[b]*Centro de Investigación Biomédica en Red sobre Enfermedades Neurodegenerativas* (*CIBERNED*), *Spain*
[c]*Dpto. Bioquímica y Biología Molecular, Facultad de Farmacia Universidad de Sevilla, Spain*
[d]*Instituto de Biomedicina de Sevilla* (*IBiS*)*-Hospital Universitario Virgen del Roc ío/CSIC/Universidad de Sevilla, Spain*
[e]*Servicio de Neurología, Hospital Universitario Virgen de la Victoria, Málaga, Spain*

Handling Associate Editor: Justo Garcia de Yebenes

Accepted 22 February 2010

Abstract. Specific neuronal networks are preferentially affected in the early stages of Alzheimer's disease (AD). The distinct subpopulations of hippocampal inhibitory GABAergic system have been shown to display differential vulnerability to neurodegeneration in AD. We have previously reported a substantial loss of SOM/NPY interneurons, whereas those expressing parvalbumin were unaltered, in the hippocampus of 6 month-old PS1/AβPP transgenic mice. In the present study, we now investigated the pathological changes of hippocampal calretinin (CR) interneurons in this PS1/AβPP model from 2 to 12 months of age. The total number of CR-immunoreactive inhibitory cells was determined by stereology in CA1 and CA2/3 subfields. Our findings show a substantial decrease (35%–45%) of CR-positive interneurons in both hippocampal subfields of PS1/AβPP mice at very early age (4 months) compared to age-matched control mice. This decrease was accompanied by a reduced CR mRNA content as determined by quantitative RT-PCR. However, the number of another hippocampal CR-positive population (belonging to Cajal-Retzius cells) was not affected. The selective early loss of CR-interneurons was parallel to the appearance of extracellular Aβ deposits, preferentially in CR-axonal fields, and the formation of dystrophic neurites. This specific GABAergic subpopulation plays a crucial role in the generation of synchronous rhythmic activity in hippocampus by controlling other interneurons. Therefore, early alterations of hippocampal inhibitory functionality in AD, caused by select CR-cells neurodegeneration, could result in cognitive impairments seen in initial stages of the disease.

Keywords: Alzheimer's disease, amyloid, hippocampal formation, inhibitory neurons, neurodegeneration, neuropathology, transgenic

INTRODUCTION

Transgenic mice overexpressing mutant familial Alzheimer's disease (AD) genes [amyloid-β protein precursor (AβPP), presenilin-1 (PS1), and PS2] are widely used to study AD-related pathology progres-

[1]These authors contributed equally to this work.

*Correspondence to: Antonia Gutierrez, PhD, Dept. Biología Celular, Genética y Fisiología, Facultad de Ciencias, Universidad de Málaga, Campus de Teatinos, 29071, Málaga, Spain. Tel.: +34 952133344; Fax: +34 952131937; E-mail: agutierrez@uma.es.

ISSN 1387-2877/10/$27.50

sion and the mechanisms underlying neuronal dysfunction [1,2]. However, the pathogenesis of AD is highly complex and these mice display some, but not all, neuropathological lesions of the disease. The most relevant discrepancy is the scarce or delayed neuronal loss in AD models concomitant with the accumulation of extracellular/intracellular amyloid-β (Aβ). We have recently reported a significant entorhinal principal cell loss in 6 month-old PS1^{M146L}/AβPP751^{SL} mice that was induced by extracellular, not intracellular, Aβ accumulation [3]. This early principal cell neurodegeneration in the entorhinal cortex was previous to that seen in hippocampus (18 months) as described in AD patients. Moreover, both brain areas in this transgenic mice display a prominent early reduction of SOM/NPY interneurons of GABA system [3,4] as occurs in AD brains [5–12]. Therefore, this PS1/AβPP mouse could mimic the initial stages of the pathology in humans and could be of great interest to analyze the age-dependent vulnerability of different neuronal subpopulations to this disease.

Neurons expressing the calcium binding protein calretinin have also been reported to be affected in the most degenerated brain regions of AD patients [13,14]. Briefly, the density of calretinin (CR) neurons, as well as the dendritic immunostaining, was reduced in the entorhinal cortex of severe AD cases [14]. The presence of CR-positive dystrophic neurites has been reported in AD hippocampus, though the number of CR-cells seemed to be preserved [13]. Some studies have reported the resistance of CR neocortical neurons to degeneration in AD [15,16], however, a layer specific vulnerability of CR-cells associated with the presence of neurofibrillary tangles has been shown in AD neocortex [17]. So far, no study has examined the viability of CR interneurons in an AD model. Therefore, the aim of the current study was to extend our previous results about interneuron vulnerability in AD by evaluating if calretinin interneurons were also affected in the hippocampal formation of our PS1/AβPP model at early stages of Aβ pathology. This CR-positive GABAergic subpopulation plays a crucial role in the hippocampal activity by controlling other interneurons terminating on different dendritic and somatic compartments of principal cells [18–20]. Here, we have quantitatively determined, by immunohistochemistry and stereological approaches, the number of CR immunoreactive interneurons in CA1 and CA2/3 subfields of 2, 4, 6, and 12 month-old PS1/AβPP mice hippocampus compared to wild type (WT) and single transgenic PS1 littermates. In addition, the CR mRNA content of the hippocampus was assessed by quantitative RT-PCR. As early as 4 months of age, coinciding with the onset of extracellular Aβ pathology, the cell number of this specific interneuron population, as well as the CR mRNA level, was significantly reduced in the double transgenic AD model.

MATERIALS AND METHODS

Transgenic mice

Male transgenic mice expressing familial AD-causing mutations in the PS1 and AβPP genes were used in this study. The PS1^{M146L}/AβPP751^{SL} mice were obtained by crossing homozygous PS1 mice (expressing human mutant PS1[M146L] under HMG-CoA reductase promoter) to hemizygous AβPP751^{SL} mice (expressing human mutant AβPP751 carrying the Swedish [KM670/671NL] and London [V717I] mutations under the control of the Thy1 promoter). Transgenic mice were generated at the Sanofi-Aventis Centre de Recherche de Paris (Vitry sur Seine, France). The generation and initial characterization of these mice has been reported previously [4,21–23]. The control group included single PS1^{M146L} transgenic mice and non-transgenic mice (WT) of the same genetic background (C57BL/6) and age. Animals of 2-, 4-, 6-, and 12-months of age for each genotype (PS1^{M146L}/AβPP751^{SL}, PS1^{M146L}, and WT) were used. All animal experiments were carried out in accordance with the European Union regulations (Council Directive 86/609/EEC of 24 November 1986) and approved by the committee of animal use for research at Malaga University, Spain (RD 1201/2005 of 10 October 2005).

Tissue preparation

After deep anesthesia with sodium pentobarbital (60 mg/kg), 2, 4, 6, and 12-month-old WT, PS1, and PS1/AβPP transgenic mice were perfused transcardially with 0.1 M phosphate-buffered saline (PBS), pH 7.4 followed by 4% paraformaldehyde, 75 mM lysine, 10 mM sodium metaperiodate in 0.1 M phosphate buffer (PB), pH 7.4. Brains were post-fixed overnight in the same fixative solution at 4°C, cryoprotected in 30% sucrose, sectioned at 40 μm thickness in the coronal plane on a freezing microtome and serially collected (each series contained sections that represented 1/7th of the total brain) in cold PBS and 0.02% sodium azide.

Immunohistochemistry

Serial sections from PS1/AβPP, PS1, and WT mice were assayed simultaneously for light microscopy immunohistochemistry as previously reported [3,4]. Briefly, free-floating sections were first pretreated with 3% H_2O_2/3% methanol in PBS and with avidin-biotin Blocking Kit (Vector Labs, Burlingame, CA, USA). For single immunolabeling, sections were incubated overnight at room temperature with one of the following primary antibodies: rabbit polyclonal anti-calretinin (1:5000 dilution; Swant), mouse monoclonal anti-Aβ 6E10 (1:1500 dilution; Sigma), or mouse monoclonal anti-reelin (1:1000 dilution; Chemicon). The tissue-bound primary antibody was detected by incubating with the corresponding biotinylated secondary antibody (1:500 dilution, Vector Laboratories), and then followed by 1:2000 streptavidin-conjugated horseradish peroxidase (Sigma Aldrich). The peroxidase reaction was visualized with 0.05% 3-3'-diaminobenzidine tetrahydrochloride (DAB), 0.03% nickel ammonium sulphate, and 0.01% hydrogen peroxide in PBS. Sections were then mounted onto gelatin-coated slides, dehydrated in graded ethanol, cleared in xylene and coverslipped with DPX (BDH) mounting medium. The specificity of the immune reactions was controlled by omitting the primary antisera.

For double CR/NeuN immunoperoxidase labeling, sections were first immunolabeled with anti-CR using DAB/nickel to visualize the reaction product (blue end product), and then processed for NeuN immunostaining (anti-NeuN monoclonal antibody, 1:1000 dilution; Chemicon) using only DAB as chromogen (brown end product). For double CR/reelin and CR/SMI312 (1:50000 dilution; Covance) immunofluorescence labelings, sections were sequentially incubated with the indicated primary antibodies followed by anti-rabbit Alexa488 secondary antibody (1:1000 dilution; Invitrogen), anti-mouse biotinylated secondary antibody (1:500; Vector Laboratories), and streptavidin-conjugated Alexa568 (1:2000 dilution; Invitrogen). For double NeuN/Propidium iodide fluorescence labeling, sections were first immunolabeled for NeuN using an anti-mouse Alexa488 (1:1000 dilution; Invitrogen) as secondary antibody and then counterstained with propidium iodide (4 μg/ml). Sections were then mounted onto gelatin-coated slides, coverslipped with 0.01M PBS containing 50% glycerin and 2.5% triethylenediamine and then examined under a confocal laser microscope (Leica TCS-NT).

Stereological analysis

Immunopositive cells for calretinin (CR-positive interneurons and CR-positive Cajal-Retzius population) belonging to the different animal groups (WT, PS1, and PS1/AβPP) and ages (2, 4, 6, and 12 months) were quantified ($n = 5$ per genotype and age; 10–12 sections per animal) in the hippocampal formation (CA1 and CA2/3 subfields) according to the optical fractionator method as previously described [3,4]. Reelin-positive Cajal-Retzius cells at the hippocampal fissure were counted at 6 months of age ($n = 5$ per genotype; 10–12 sections per mouse). Double labeled CR/NeuN cells as well as total NeuN-positive cells were quantified in the stratum radiatum of 4 month-old animals ($n = 4$ per genotype; 10–12 sections/mouse). In addition, total NeuN-positive cells were counted in the stratum radiatum of 2 month-old mice ($n = 4$ per genotype; 10–12 sections/mouse). Briefly, an Olympus BX61 microscope and the NewCAST software package (Olympus, Glostrup, Denmark) were used. The number of neurons was quantified in every 7th section (with a distance of 280 μm between sections) through the entire antero-posterior extent of the hippocampus (between -0.94 mm anterior and 3.64 mm posterior to Bregman) according to the atlas of Franklin and Paxinos [24]. CA1 and CA2-3 subfields were defined using a 10x objective and the number of neurons was counted using a 100X/1.35 objective. The number of counting frames varied with the hippocampal region or subfield layer analyzed. We used a counting frame of 1874.2 μm^2 with step lengths of 78.93 $\times$ 78.93 μm for CR and reelin counting, and another of 941.42 μm^2 with step lengths of 49.47 $\times$ 37.25 μm for NeuN and double CR/NeuN counting. The total cell number was estimated using the optical fractionator formula, $N = 1/ssf.1/asf.1/hsf.\sum Q^-$, where *ssf* represents the section sampling fraction, *asf* is the area sampling fraction, which is calculated by dividing the area sampled with the total area of the layer, *hsf* stands for the height sampling fraction, which is calculated by dividing the height sampled (10 μm in this study) with the section thickness, and $\sum Q^-$ is the total count of nuclei sampled for the entire layer [25–27]. The precision of the individual estimations was expressed by the total coefficient of error (CE) [28] calculated using the CEs in each individual animal. The CEs ranged between 0.01 and 0.07. An investigator who was blind to the experimental conditions (age, genotype, and marker) performed neuronal profile counting.

Plaque loading

Quantification of extracellular Aβ content was performed as previously reported [22]. Briefly, 6E10 immunostained PS1xAβPP sections (seven sections/mouse; $n = 5$ per age) were observed under a Nikon Eclipse 80i microscope using a 4x objective and images acquired with a Nikon DS-5M high-resolution digital camera. Digital images were analyzed using Visilog 6.3 analysis program (Noesis, France). Plaque loading was defined as percentage of total hippocampal area stained for Aβ excluding principal cell layers intracellular labeling that was removed by manual editing. The hippocampal area in each 4 $\times$ image was manually outlined. The plaque loading (%) for each mouse was estimated and defined as (sum plaque area measured/sum hippocampal area analyzed) $\times$ 100. The sums were taken over all slides sampled and a single plaque burden was computed for each mouse.

RNA and total protein extraction

Anaesthetized mice ($n = 8$ per genotype and age) were killed by decapitation and both hippocampi were dissected, frozen in liquid nitrogen, and stored at $-80°$C until use. Total RNA was extracted using the Tripure^{TM} Isolation Reagent (Roche) as described previously [3,4,23]. The contaminating DNA in the RNA samples was removed by incubation with DNAase (Sigma-Aldrich) and confirmed by PCR analysis of total RNA samples prior reverse transcription. After isolation, the integrity of the RNA samples was assessed by agarose gel electrophoresis. The yield of total RNA was determined by measuring the absorbance (260/280 nm) of ethanol-precipitated aliquots of the samples. The recovery of RNA was comparable in all groups (1.2–1.5 μg/mg of tissue). The protein pellets, obtained using the Tripure^{TM} Isolation Reagent, were resuspended in 4% SDS and 8M urea in 40 mM Tris-HCl, pH 7.4 and rotated overnight at room temperature.

Retrotranscription and real-time RT-PCR

The retrotranscription (RT) was done using random hexamers, 3 μg of total RNA as template and High-Capacity cDNA Archive Kit (Applied Biosystems) following the manufacturer recommendations [4,22,23]. For real time RT-PCR, gene product was amplified using commercial Taqman^{TM} probes, following the instruction of the manufactured (Applied Biosystems), using an ABI Prism 7000 sequence detector (Applied Biosystems). A standard curve was first constructed, using increasing amounts of cDNA. The slope of the curve indicated optimal PCR conditions (slope 3.2–3.4). The cDNA levels of the different mice were determined using two different housekeepers (i.e., GAPDH and β-actin). The amplification of the housekeepers was done in parallel with the gene to be analyzed. Similar results were obtained using both housekeepers. Thus, the results were normalized using only the GAPDH expression. Results were always expressed using the comparative Ct method, following the Bulleting number 2 from Applied Biosystems. As a control condition, we selected 4-month-old WT mice. In consequence, the expression of the tested gene, for all ages and mice types, was referenced to the expression levels observed in 4-month-old WT mice.

Statistical analysis

Data was expressed as mean $\pm$ SD. The comparisons between several groups (WT, PS1, and PS1/AβPP mice) and ages (2, 4, 6, and 12 months) were done by one-way ANOVA followed by Bonferroni post hoc multiple comparisons test, and those between two mice groups by two-tailed t-test (SigmaStat® 2.03, SPSS Inc). In both cases, the significance was set at 95% of confidence.

RESULTS

The number of hippocampal CR-interneurons was significantly reduced at 4 months of age coincident with the appearance of Aβ deposits

In order to determine the number of CR interneurons in hippocampal CA1 and CA2/3 regions of PS1/AβPP, PS1, and WT mice at 2, 4, 6, and 12 months of age, we have combined specific CR immunohistochemical detection with unbiased stereological cell counting method. The immunohistochemical examination of WT sections revealed CR-positive cells in all layers (more often in principal cell layer) of CA1 regions with multipolar and bipolar or fusiform somata as previously described [29]. Most of these interneurons possessed two dendrites that ran radially and transversed several hippocampal layers (Fig. 1A). Similar observations (cell morphology and spatial location) were done in transgenic mice sections at 2 months of age (Fig. 1B), however, a reduced number of CR-positive cells in the CA subfields in PS1/AβPP animals was observed since

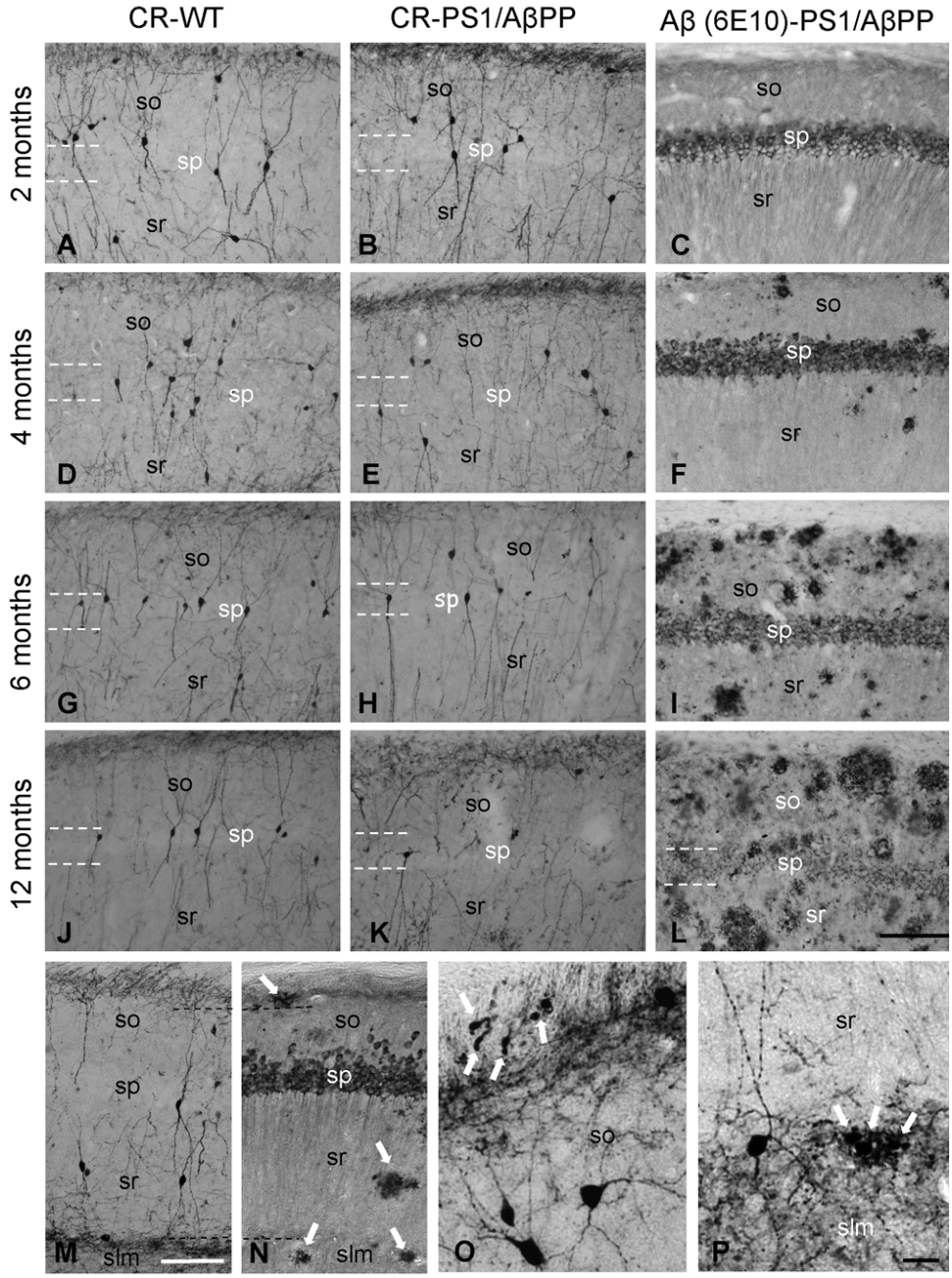

Fig. 1. CR-immunoreactive interneurons in hippocampal CA1 subfield. Light microscopic images of CR immunoreactivity in CA1 subfield of WT (A-D-G-J) and PS1/AβPP (B-E-H-K) mice at 2, 4, 6, and 12 months of age. CR-cells are located in all layers. These cells have smooth or beaded radially oriented dendrites. A decrease in the density of CR-positive cells was observed in PS1/AβPP mice compared to WT mice since 4 months of age. The reduction of CR-positive cells was associated with the apparition of Aβ extracellular deposition (C-F-I-L). CR-positive plexi were located at stratum oriens/alveus border and in the stratum lacunosum-moleculare (M) where extracellular Aβ deposits (arrows) were preferentially detected since 4 months of age (N). The presence of CR-positive dystrophic neurites (arrows) was observed in the stratum oriens/alveus (O) and stratum lacunosum-moleculare (P) CR-positive terminal fields at 4 months of age. so: stratum oriens; sp: stratum pyramidale; slm: stratum lacunosum-moleculare; sr: stratum radiatum. Scale bars: 100 μm (A-L, M and N); 25 μm (O and P).

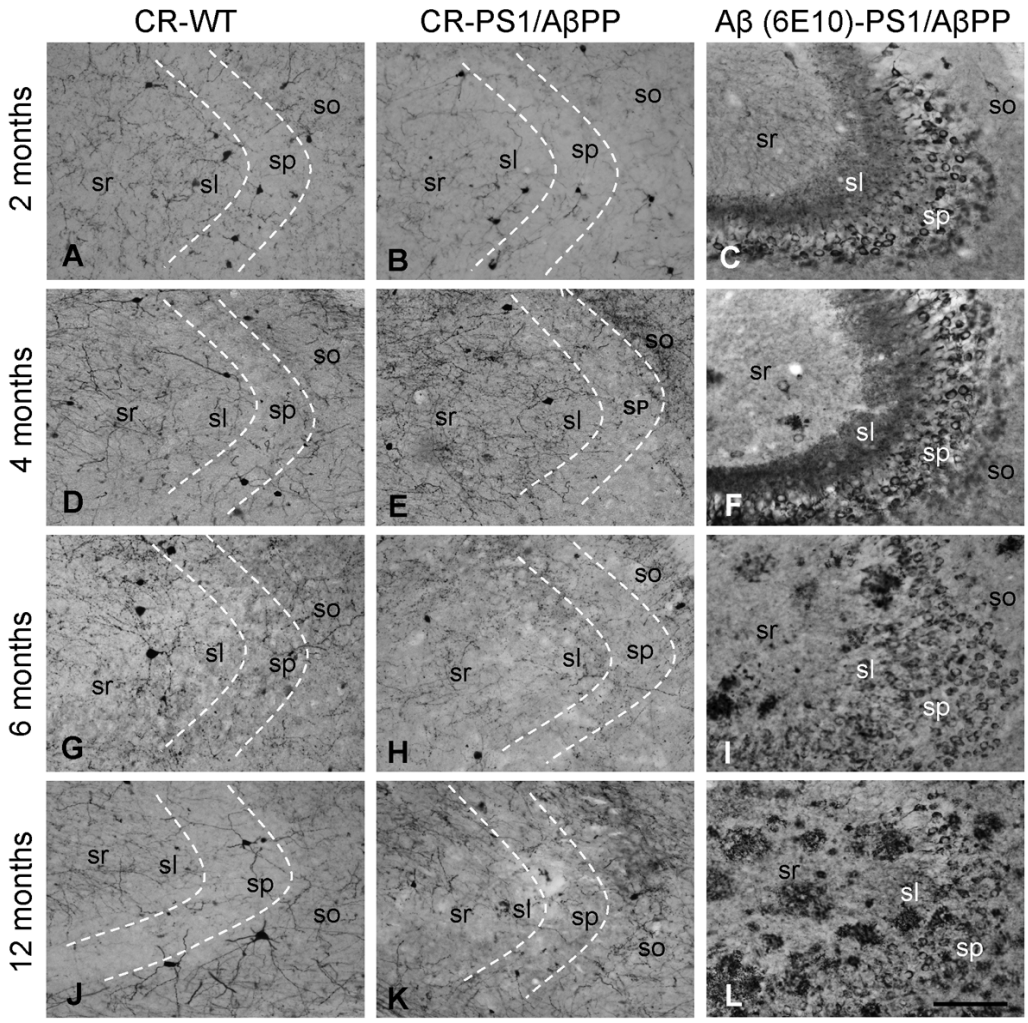

Fig. 2. CR-immunoreactive interneurons in hippocampal CA3 subfield. Light microscopic images of CR-immunoreactivity in CA3 subfield of WT (A-D-G-J) and PS1/AβPP (B-E-H-K) mice at 2, 4, 6, and 12 months of age. Most of CR-cell bodies were in strata oriens and radiatum. The number of CR-positive cell bodies was reduced in PS1/AβPP mice compared to WT mice since 4 months of age. Parallel to the decrease of CR-positive cells there was an increase in the number and size of Aβ deposits (C-F-I-L). so: stratum oriens; sp: stratum pyramidale; sl: stratum lucidum sr: stratum radiatum. Scale bar: 100 μm.

4 months of age (Fig. 1E, H, and K) compared to age-matched WT (Fig. 1D, G, and J) or PS1 (not shown) animals. In CA2/3 subfield, the CR-immunoreactive pattern in WT animals was also consistent with earlier descriptions, seeing many CR-positive cells, mainly in strata pyramidale, lucidum, and radiatum (Fig. 2A and D). Double transgenic mice displayed same CR-immunoreactive pattern (Fig. 2B) though, as seen for CA1 subfield, the number of CR-cells was reduced since 4 months of age (Fig. 2E, H and K) in comparison with non-transgenic (Fig. 2D, G and J) or PS1 mice (not shown).

The stereological quantification ($n = 5$ per genotype and age; 10–12 sections/animal) showed a significant (one-way ANOVA $p < 0.001$, Bonferroni post-hoc multiple comparison test) reduction in the total number of CR-cells in CA1 ($44 \pm 11.45\%$, $p < 0.001$) and CA2-3 ($33.49 \pm 4.48\%$, $p < 0.01$) subfields of PS1/AβPP mice at 4 months of age compared to WT and PS1 littermates (Fig. 3A and B). At 6 months of age, the decrease in CA1 was $45.75 \pm 14.63\%$ ($p < 0.001$) and in CA2-3 of $38.79 \pm 11.74\%$ ($p < 0.05$). Later, at 12 months of age, CA1 and CA2/3 displayed $38.45 \pm 7.40\%$ ($p < 0.05$) and $37.70 \pm 2.84\%$ ($p < 0.05$) reduction respectively. An age-dependent decrease (one-way ANOVA, Bonferroni $p < 0.05$) in CR-

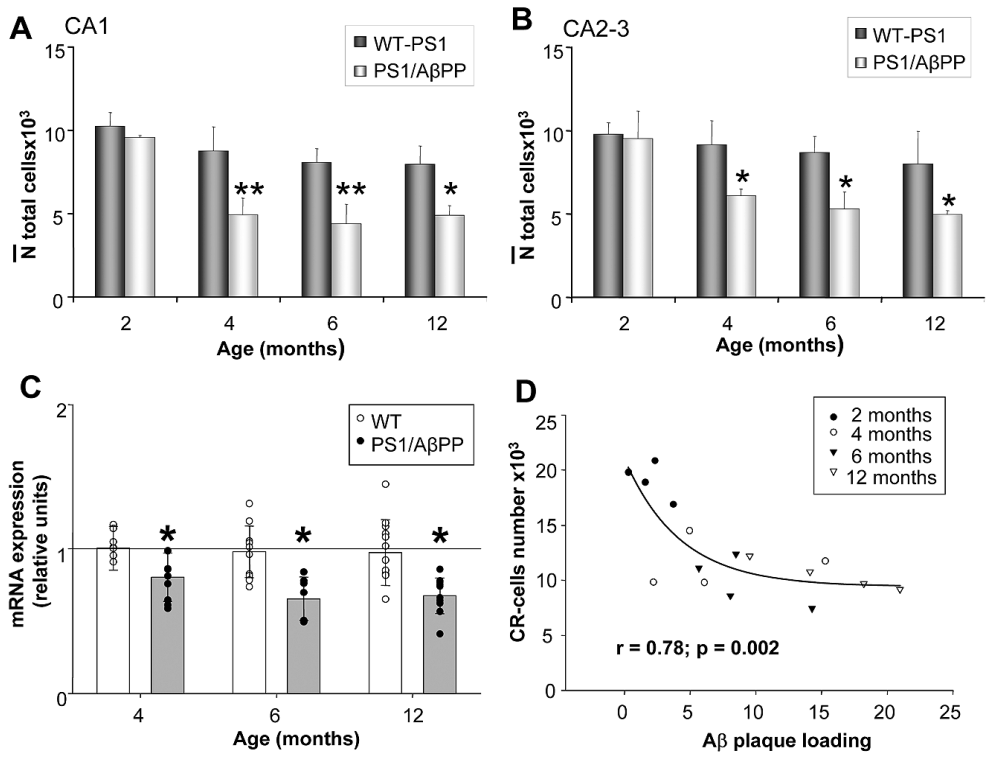

Fig. 3. Significant reduction of CR-interneurons in PS1/AβPP hippocampal formation at early ages. Stereological quantification of CR-positive cells in WT-PS1 and PS1/AβPP ($n = 5$ per genotype and age) demonstrated a significant decrease in PS1/AβPP compared to WT-PS1 mice since 4 months of age in both CA1 (A) and CA2/3 (B) subfields. Data (mean $\pm$ SD) was analyzed by one-way ANOVA $p < 0.001$ (CA1 F(7,27) $= 28.72$ and CA2-3 F(7,28) $= 11{,}69$), followed by Bonferroni post-hoc multiple comparison test. Significance (**$p < 0.001$, *$p < 0.05$) was indicated in the figure. No differences were detected between PS1 and WT animals and data were pooled. C) CR cells were quantitatively determined in the hippocampus of PS1/AβPP and WT-PS1 mice by RT-PCR ($n = 8$ per genotype and age). The expression of CR mRNA was significantly decreased in PS1/AβPP mice since 4 months of age compared to age-matched control groups. This quantification corresponded to all hippocampal CR cells subpopulations including interneurons, Cajal-Retzius cells, mossy cells and subgranular new born CR expressing neurons. Data (mean $\pm$ SD) was analyzed by one-way ANOVA $p = 0.0001$ (F(5,54) $= 6.5$) followed by Bonferroni post-hoc multiple comparison test. Significance (*$p < 0.05$) was indicated in the figure. D) An inverse biphasic correlation was found between the number of CR-interneurons and the extracellular Aβ content within same PS1xAβPP animals. This relationship was not linear as Aβ load progressively increased with age whereas CR-cells reduction remained constant after 4–6 months of age.

interneurons number in CA1 region of control animals was detected at 6 ($21.09 \pm 7.77\%$) and 12 months ($22.41 \pm 10.59\%$) of age, compared to 2 months group (Fig. 3A). In CA2/3 region this decrease in WT animals with age was also observed (Fig. 3B) though it did not reach statistical significance. The number of CR interneurons remained unchanged between PS1 transgenic mice and WT mice of same age in CA subfields and data were pooled. Importantly, no differences between PS1/AβPP and WT-PS1 mice were observed at 2 month-old.

Furthermore, we found a similar decrease in the CR mRNA content in PS1/AβPP hippocampus at 4 months of age as assessed by quantitative real time RT-PCR (Fig. 3C). This reduction was of $20.2 \pm 16.7\%$ ($p < 0.05$), $34.6 \pm 15.0\%$ ($p<0.05$), and $32.4 \pm 12.3\%$ ($p < 0.05$) at 4, 6, and 12 month of age, respectively (one-way ANOVA $p = 0.0001$, Bonferroni post-hoc; $n = 8$ per genotype and age). The assessed mRNA expression accounts for total hippocampal CR-cell populations, including interneurons, Cajal-Retzius cells, hilar mossy cells and subgranular newly born neurons that transiently express CR. Besides this CR-cell heterogeneity there was not much difference between this mRNA quantitative assays and the stereological interneuron counts, indicating that this subpopulation is the most affected one among CR-cells. In fact, and despite that different groups of animals were used for stereological counting and mRNA assays, a good correlation was found between the decrease in both parameters in this AD model (not shown).

The progression of Aβ pathology was determined by 6E10 immunostaining in adjacent sections of the same PS1/AβPP animals (Figs 1 and 2C, F, I, and L). This monoclonal antibody recognizes Aβ as well as the precursor protein AβPP. Results showed intense intracellular immunolabeling of pyramidal cell bodies and proximal dendrites at early ages (2 and 4 months) and then intensity diminished with age (more patent at 12 months). However, no immunoreactivity was observed within interneuronal cell bodies at any age tested. Thus, as expected no Aβ expression or accumulation occurs in hippocampal GABAergic cells in this model. Interestingly, extracellular Aβ deposits were already detected at 4 months of age, coinciding with the decrease in the number of CR-cells in CA subfields. The apparition of Aβ deposits has been documented to start at 2.5–3 months of age in this transgenic model [21]. In the hippocampal formation the Aβ deposits were mainly located in the CR-axonal terminal fields such as stratum lacunosum-moleculare and stratum oriens/alveus boundary (see Fig. 1M and N). The presence of CR-positive dystrophic neurites in both axonal fields was detected since 4 months of age (Fig. 1O and P). These CR-positive dystrophic neurites which were immunoreactive for SMI312 antibody against phosphorylated neurofilaments (not shown) displayed a swollen/globular appearance and were preferentially located around plaques (identified by Congo red staining). The number and size of extracellular deposits, significantly increased with age, as previously reported [23], and this was accompanied by an increase in the number of dystrophic neurites. Therefore, the decrease in the number of CR-positive interneurons seemed to be associated with extracellular, not intracellular, Aβ accumulation. In support of this, an inverse correlation between CR-cell number and Aβ plaque loading was found (Fig. 3D). As also expected, the correlation between both parameters was not linear, since the Aβ loading increased with the age of the animal whereas the CR-cell number, after the initial decrease (from 2 to 6 months) remained practically constant. A similar biphasic response was also observed for hippocampal GABAergic SOM-positive cells in this AD model (unpublished results).

In contrast to CR-interneurons, the CR-positive Cajal-Retzius cells were not affected by extracellular Aβ pathology

A CR-positive population with small round somata was found in the outer third of the molecular layer and inner part of the lacunosum-moleculare at the hippocampal fissure (Fig. 4A1-A4). These CR-cells corresponded to Cajal-Retzius neurons which coexpress reelin [30] (Fig. 4B1 and B2) as seen in double CR/reelin immunofluorescence labeling (Fig. 4C). However, not all reelin-positive Cajal-Retzius cells expressed CR (Fig. 4C). The stereological study for CR-positive Cajal-Retzius cells (from 2 to 12 months) showed no differences between control (WT-PS1) and PS1/AβPP groups ($n = 5$ per genotype and age) at any age tested (Fig. 4D). Moreover, the total number of reelin-positive Cajal-Retzius cells at the hippocampal fissure did not display any change between genotypes either (at 6 months the values were 14672.82 ± 58.98 cells for PS1/AβPP mice versus 13462.13 ± 544.63 cells for the control group; $n = 5$ per genotype). However, a significant (one way ANOVA $p < 0.001$, Bonferroni post-hoc) reduction during aging in the total number of CR-positive Cajal-Retzius population was observed in all genotypes (Fig. 4D). This reduction was quite similar for PS1/AβPP ($45.10 \pm 8.54\%$, $57.43 \pm 11.13\%$, $80.49 \pm 23.34\%$ at 4, 6, and 12 months respectively) and control (WT-PS1) animals ($40.26 \pm 8.64\%$, $57.77 \pm 15.43\%$, $80.19 \pm 26.54\%$ at 4, 6, and 12 months respectively) compared to their corresponding 2 month-old group. No differences between PS1 and WT mice were observed and data were pooled. Then, CR-positive Cajal-Retzius cells were equally affected by age in the hippocampus of WT, PS1, and PS1/AβPP mice. These cells were not specifically affected by Aβ pathology in PS1/AβPP animals. These findings emphasize the selective early vulnerability of CR-positive interneurons compared to other CR-cells in this AD model.

The reduced number of CR-positive interneurons was consequence of an early neurodegenerative process

To determine whether the early reduction of CR-positive interneurons in PS1/AβPP hippocampus reflects neuronal loss or an altered phenotype (loss of CR expression), we have performed parallel stereological counts of CR-positive cells and the total neuronal population in the stratum radiatum of CA1 by using double CR-NeuN peroxidase immunolabeling (Fig. 5A and B). The immunoreaction with the antibody to CR labeled the cytoplasm of this interneuron subpopulation in dark blue color whereas the second immunostaining using anti-NeuN labeled all neuronal nuclei in light brown color. All neurons in strata radiatum and oriens are GABAergic inhibitory neurons, however, the

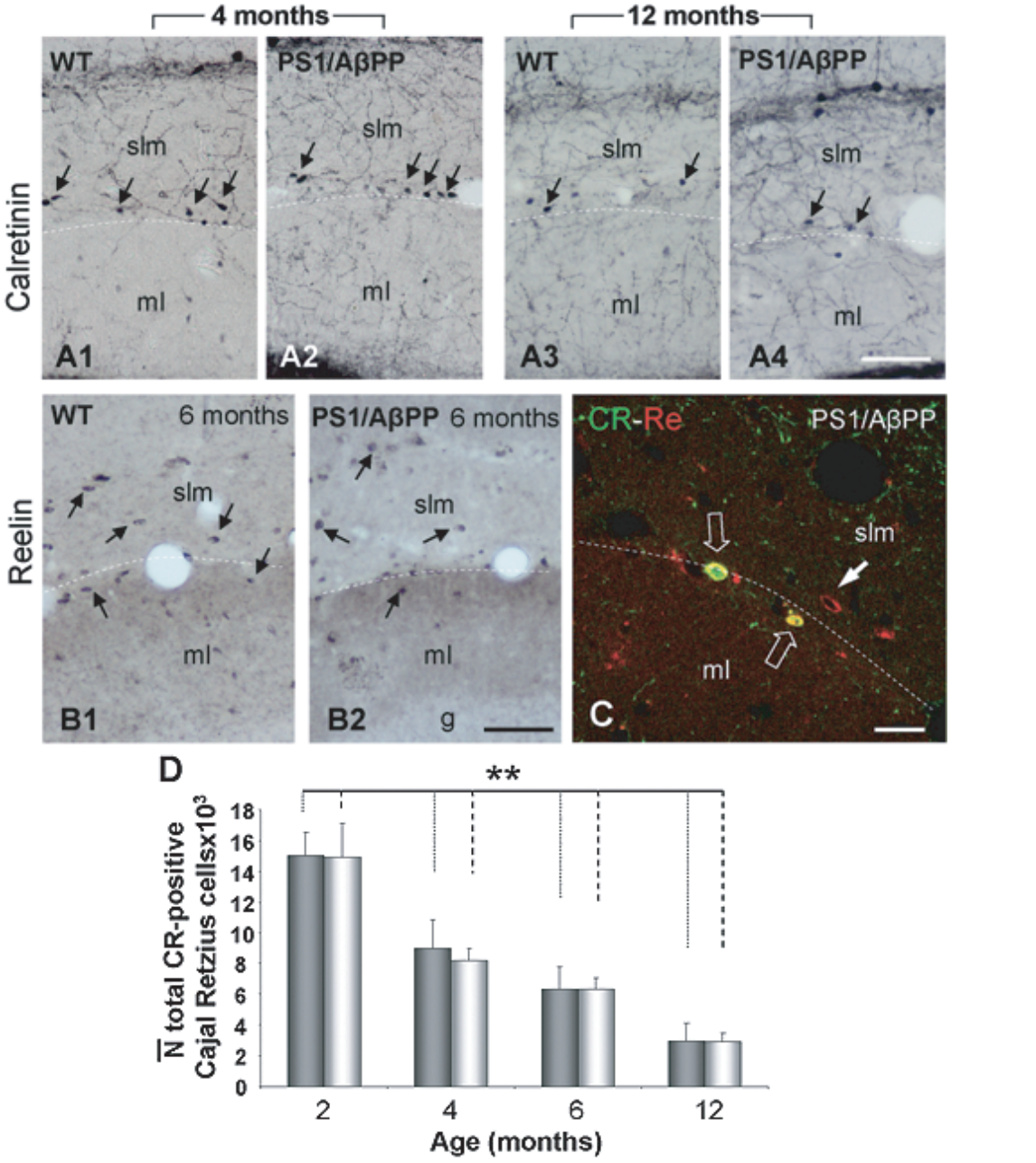

Fig. 4. CR-positive Cajal-Retzius cells are not affected by Aβ pathology. A) Light microscopy images of CR-positive cells (arrows) in hippocampal fissure of WT (A1 and A3) and PS1/AβPP (A2 and A4) mice at 2 (A1-A2) and 12 (A3-A4) months of age. B) Light microscopy images of Cajal-Retzius cells immunoreactive for reelin (arrows) in the hippocampal fissure of WT (B1) and PS1/AβPP (B2) mice demonstrated no qualitative differences between both genotypes at 6 months of age. C) Double immunofluorescence confocal laser scanning image for CR (green) and reelin (red) in PS1/AβPP hippocampal fissure at 6 months of age. CR-cells also expressed reelin (open arrows), however some reelin-positive cells were CR-negative (white arrow). D) No differences were detected between PS1/AβPP and WT-PS1 control groups ($n = 5$ per genotype and age) in the number of CR-positive Cajal-Retzius cells at all ages tested. However, a significant age-dependent reduction in the number of these cells was found in both PS1 and WT-PS1 groups since 4 months when compared to 2 month-old mice. Data (mean $\pm$ SD) were analyzed by one-way ANOVA $F(7,23) = 45{,}33$, followed by Bonferroni post-hoc multiple comparison test. Significance $^{**}p < 0.001$ was indicated in the figure. slm: stratum lacunosum-moleculare; ml: molecular layer; g: granular cell layer; Re: reelin. Scale bars: 100 μm (A1-A3, B1 and B2); 20 μm (C).

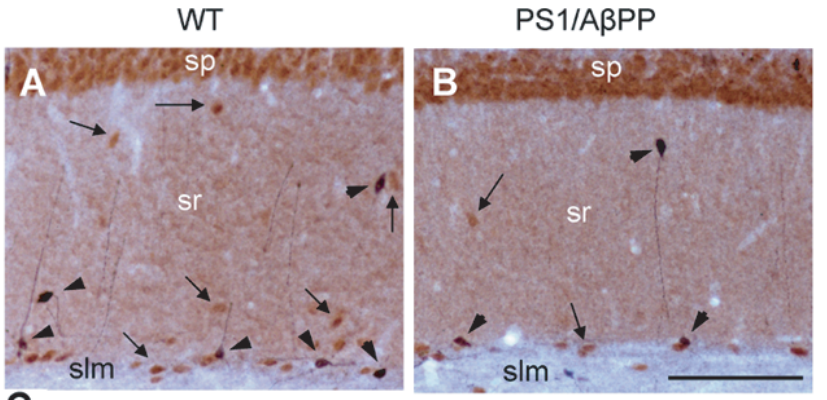

C

N total cells				
			Difference from WT-PS1	
	NeuN	CR	NeuN	CR
WT-PS1	4621.2 ± 439.7	1324.2 ± 83.8	-	-
PS1/AβPP	**3567.6 ± 411.9***	**1034.3 ± 36.4***	989.1 ± 305.1	289.9 ± 47.5

two tailed t-test, *p<0.05

Fig. 5. Loss of CR-positive interneurons in PS1/AβPP hippocampus is due to a neurodegenerative process. A,B) Bright field microscopy images of double peroxidase immunolabeling for CR (dark blue) and NeuN (brown) in CA1 stratum radiatum of 4 month-old WT (A) and PS1/AβPP (B) mice. A reduced number of NeuN-positive cells (arrows) as well as CR-immunoreactive cells (arrowheads) was found in stratum radiatum of PS1/AβPP mice compared to WT. C) Stereological quantification of NeuN- and CR/NeuN-positive cells in CA1 stratum radiatum demonstrated a significant (two tailed t-test, *$p < 0.05$) decrease for NeuN-positive cells (22.79 $\pm$ 10.15%) and for CR-interneurons (21.89 $\pm$ 9.78%) in 4 month-old PS1/AβPP ($n = 4$) compared to age-matched WT-PS1 ($n = 8$) mice. However, the loss of CR-positive interneurons, calculated as the difference between WT-PS1 and PS1/AβPP cell numbers, represented one third of the NeuN cell loss. so: stratum oriens; sp: stratum pyramidale; sr: stratum radiatum; slm: stratum lacunosum-moleculare. Scale bar: 100 μm.

stratum radiatum has been reported to contain higher proportion of CR interneurons than stratum oriens [31]. Stereological counts (Fig. 5C) showed that the loss of CR-positive cells (21.89 $\pm$ 9.78%, two tailed t-test p<0.005) was quite similar to the NeuN-positive neurons (22.79 $\pm$ 10.15%, two tailed t-test $p < 0.05$) in PS1/AβPP ($n = 4$) respect to age-matched WT-PS1 ($n = 8$) animals at 4 months of age. However, the loss of the CR cells calculated as the difference between WT-PS1 and PS1/AβPP (Fig. 5C) represented only one third of the NeuN-positive cell loss (289.9 $\pm$ 47.5 CR cells versus 989.1 $\pm$ 305.1 NeuN cells), indicating that other(s) interneuronal population(s), probably SOM/NPY interneurons as previously reported by our group [4], are also affected in this layer. To discard the possibility of early-developmental neuronal deficits in transgenic animals, we have performed stereological counts in the stratum radiatum at 2 months of age. Results showed that the number of NeuN-positive cells in the stratum radiatum (interneurons) of PS1/AβPP mice was not significantly different from age-matched controls (97.38 $\pm$ 3.16% compared to 2 month-old control group, $n = 4$/genotype), which further proved that neuronal loss in 4 month-old PS1/AβPP mice was most likely due to neurodegeneration. Moreover, to avoid the possibility that interneuron decrease in 4 month-old double transgenic mice reflected a loss of NeuN-epitope, instead cell death, we have also used a non-immunohistochemical method (fluorescent DNA marker propidium iodide) for cell identification along with NeuN-immunostaining. Although we have not performed stereological count of these double fluorescent labeled sections, the analysis of confocal images (6 sections/mouse, $n = 3$ mice/age) have not revealed propidium iodide-labeled neuronal nuclei (identified by morphological criteria) which were NeuN-negative in PS1/AβPP mice hippocampus at 2 and 4 months of age (results not shown).

Taken together, all these data support the existence of a neurodegenerative process in PS1/AβPP hippocampus at early ages.

DISCUSSION

Select neuronal populations display different sensitivity to degeneration in aging and AD pathology. In this study we have extended our previous results on GABAergic interneuron vulnerability in PS1/AβPP transgenic AD model and demonstrated: 1) a significant reduction (35–45%) in the total number of CR-interneurons in CA1 and CA2/3 hippocampal subfields of PS1/AβPP mice at 4 months of age which was also reflected by a reduced CR mRNA content; 2) the neurodegeneration of CR-positive interneurons was associated to the early appearance of Aβ deposits and the formation of axonal dystrophies; and 3) this early degenerative process was selective for CR-interneurons whereas another hippocampal CR cells (CR-positive Cajal-Retzius cells) were not affected by Aβ pathology.

In the hippocampus, there is a great cellular diversity of GABAergic interneurons which provide general inhibition by contacting with distinct domains of principal cells (for review, see [32]). The different classes of inhibitory neurons can be recognized on the basis of their morphological, molecular, and physiological features. Among these GABA interneurons, those expressing the calcium binding protein calretinin represent a small percent, about 10% [31], however, they play a crucial role regulating the activity of other GABAergic inhibitory interneurons and subsequently the excitatory action of principal cells [19]. The targets of CR-axons are interneurons (containing VIP, calbindin, or somatostatin) which terminate on different somatodendritic domains of principal cells. Decrease of CR-interneurons may be then associated with functional decline of inhibitory activity in hippocampus and memory impairment. The relevance of calretinin and other calcium binding proteins in neurodegenerative diseases, and particularly AD, has been supported by several studies [13,14,33–35]. Our findings of reduced number of CR-interneurons, as well as the presence of CR-positive dystrophic neurites, in an AD model are then consistent with those observations seen in humans. Supporting the existence of altered CR networks in AD pathology, Popovic and colleagues [36] have recently reported decreased CR-immunoreactivity in the dentate gyrus hilar cells (mostly excitatory mossy cells) of another AD model.

We have demonstrated that reduction of CR-interneurons is an early event (4 months), preceding even SOM/NPY cells loss (6 months; see [4]) during disease progression in the hippocampal formation of our AD model. Our findings also show a diverse sensitivity to degeneration within the CR-interneuron population in the hippocampal formation. In particular, a subset (approximately 40% of total population) was highly susceptible whereas the rest of the population (60%) was unaffected even at late ages (there was no progressive decline in CR-positive interneurons with aging and increased Aβ pathology; see Fig. 3D). We do not know the reasons that determine this differential early vulnerability to Aβ pathology, but certainly it will be of great interest to identify the molecular/physiological properties of both CR-positive interneuronal subsets (vulnerable/resistant) to uncover the underlying mechanisms that lead to neurodegeneration/survival. Nevertheless, the loss of this vulnerable CR-interneuron subset could be responsible, in part, of first signs of hippocampal functional abnormalities.

Supporting the selective vulnerability of CR-interneurons, and the extensive heterogeneity among hippocampal CR-cells, we have also shown that CR-positive Cajal-Retzius cells, located in the hippocampal fissure, were not affected by the course of disease in this double transgenic mice. However, there was a substantial age-dependent reduction (reaching 80% at 12 months) of this cell population in both PS1/AβPP and control animals.

In addition, we demonstrated that the reduction of CR-interneurons in this PS1/AβPP model is due to an early neurodegenerative process rather than loss of CR-expression. Stereological analysis of double CR-NeuN immunolabeling in the stratum radiatum of CA1 subfield showed that the total number of interneuronal cells (NeuN-positive) significantly decreased at very early age (4 months). The loss of CR-cells represented 30% of the neurodegenerative process in this layer, indicating that other GABAergic neurons could also be affected. Supporting these data, we have previously demonstrated an early neurodegeneration of SOM/NPY cells in this AD model [4], however, other interneuronal populations (such as cholecystokinin positive interneurons) could be also affected (see [37]).

The mechanism underlying this early selective death of CR-interneurons remains to be elucidated, however, since hippocampal interneurons in this AD model do not express mutated hAβPP (see [4]), intracellular Aβ accumulation is not the causative neurotoxic agent. Instead extracellular factors should be the major agents involved. In this sense, we have described an association between extracellular Aβ and/or cytotoxic glial environment and the neurodegeneration of hippocampal principal cells [23] in layer V pyramidal cells of the entorhinal cortex in this PS1/AβPP

mice [3]. Supporting the direct impact of extracellular Aβ on neuronal death, Liu and colleagues [38] recently reported a relationship between forebrain extracellular Aβ accumulation and the progressive degeneration of monoaminergic afferent axons and their corresponding subcortical cell bodies. In concordance with this, we have observed abundant Aβ deposits in the CR-axonal plexi in stratum lacunosum moleculare and in stratum oriens/alveus boundary of CA1-CA3 regions at early ages in our model. Moreover, CR-positive dystrophic neurites were seen in these axonal fields. Then, we consider the possibility that extracellular Aβ could directly affect CR axon terminals and stimulate a neurodegenerative process toward their cell bodies. In fact, Aβ peptides are well established as the principal factors for the pathological events observed in AD [39–41] and there is compelling evidence showing that alterations in axonal transport play critical role in the pathogenesis of AD [42–45].

Instead of a direct neurotoxic effect of Aβ onto CR-cells, it could be also argued that Aβ might exert an indirect effect by eliciting a local cytotoxic inflammatory reaction that may in turn produce this neuronal death. In relation to this, our PS1/AβPP mice develop an extensive forebrain inflammatory response since 4 months of age, with a substantial microglial and astroglial activation [3,23]. However, the hippocampal glial activation at early ages, and on contrary to that in entorhinal cortex, might be neuroprotective and only at late ages (18 months) displayed a neurotoxic profile. Therefore, we believe that CR-positive hippocampal interneuron population is most likely affected by extracellular Aβ directly. On the other hand, we cannot excluded that death of these CR cells could be related to a deafferentation process. These interneurons receive afferents from the GABAergic component of the septohippocampal pathway and from serotoninergic raphe neurons [46]. Whether these neurons are affected in this model and precede CR-cells degeneration still need to be investigated.

In conclusion, this work provides the first evidence that hippocampal CR-interneurons are preferential early targets in a transgenic model with AD-like pathology. The loss of these GABAergic neurons may be influenced by the early onset of amyloid deposits in this brain area and the induction of axonal pathology, however, the exact molecular mechanisms responsible for this selective neurodegeneration are still unknown. Finally, our findings highlight the diversity within this neurochemically identified GABAergic population and further supports the notion that Aβ pathology affects specific neuronal subsets.

ACKNOWLEDGMENTS

This work was supported by grants PI06/0556-PS09/00099 (to AG), PI06/0567-PS09/00151 (to JV) and PI06/0781-PS09/00848 (to DR) from Fondo de Investigación Sanitaria (FIS) -Instituto de Salud Carlos III- Spain. DB-V, IM-G and SJ were the recipients of a contract from CIBERNED. RS-V, ES-M and MT held a PhD fellowship from Spain FPU or FPI programs.

Authors' disclosures available online (http://www.j-alz.com/disclosures/view.php?id=348).

REFERENCES

[1] Morrissette DA, Parachikova A, Green KN, LaFerla FM (2009) Relevance of transgenic mouse models to human Alzheimer disease. *J Biol Chem* **284,** 6033-6037.

[2] Duyckaerts C, Potier MC, Delatour B (2008) Alzheimer disease models and human neuropathology: similarities and differences. *Acta Neuropathol* **115**, 5-38.

[3] Moreno-Gonzalez I, Baglietto-Vargas D, Sanchez-Varo R, Jimenez S, Trujillo-Estrada L, Sanchez-Mejias E, Del Rio JC, Torres M, Romero-Acebal M, Ruano D, Vizuete M, Vitorica J, Gutierrez A (2009) Extracellular amyloid-beta and cytotoxic glial activation induce significant entorhinal neuron loss in young PS1M146L/APP751SL mice. *J Alzheimers Dis* **18**, 755-776.

[4] Ramos B, Baglietto-Vargas D, Del Rio JC, Moreno-Gonzalez I, Santa-Maria C, Jimenez S, Caballero C, Lopez-Tellez JF, Khan ZU, Ruano D, Gutierrez A, Vitorica J (2006) Early neuropathology of somatostatin/NPY GABAergic cells in the hippocampus of a PS1xAPP transgenic model of Alzheimer's disease. *Neurobiol Aging* **27,** 1658-1672.

[5] Beal MF, Mazurek MF, Svendsen CN, Bird ED, Martin JB (1986) Widespread reduction of somatostatin-like immunoreactivity in the cerebral cortex in Alzheimer's disease. *Ann Neurol* **20,** 489-495.

[6] Beal MF, Mazurek MF, Chattha GK, Svendsen CN, Bird ED, Martin JB (1986) Neuropeptide Y immunoreactivity is reduced in cerebral cortex in Alzheimer's disease. *Ann Neurol* **20,** 282-288.

[7] Beal MF, Benoit R, Mazurek MF, Bird ED, Martin JB (1986) Somatostatin-28(1-12)-like immunoreactivity is reduced in Alzheimer's disease cerebral cortex. *Brain Res* **368,** 380-383.

[8] Nakamura S, Vincent SR (1986) Somatostatin- and neuropeptide Y-immunoreactive neurons in the neocortex in senile dementia of Alzheimer's type. *Brain Res* **370,** 11-20.

[9] Chan-Palay V (1987) Somatostatin immunoreactive neurons in the human hippocampus and cortex shown by immunogold/silver intensification on vibratome sections: coexistence with neuropeptide Y neurons, and effects in Alzheimer-type dementia. *J Comp Neurol* **260,** 201-223.

[10] Gaspar P, Duyckaerts C, Febvret A, Benoit R, Beck B, Berger B (1989) Subpopulations of somatostatin 28-immunoreactive neurons display different vulnerability in senile dementia of the Alzheimer type. *Brain Res* **490,** 1-13.

[11] Grouselle D, Winsky-Sommerer R, David JP, Delacourte A, Dournaud P, Epelbaum J (1998) Loss of somatostatin-like immunoreactivity in the frontal cortex of Alzheimer patients

carrying the apolipoprotein epsilon 4 allele. *Neurosci Lett* **255,** 21-24.

[12] Davis KL, Mohs RC, Marin DB, Purohit DP, Perl DP, Lantz M, Austin G, Haroutunian V (1999) Neuropeptide abnormalities in patients with early Alzheimer disease. *Arch Gen Psychiatry* **56,** 981-987.

[13] Brion JP, Resibois A (1994) A subset of calretinin-positive neurons are abnormal in Alzheimer's disease. *Acta Neuropathol* **88,** 33-43.

[14] Mikkonen M, Alafuzoff I, Tapiola T, Soininen H, Miettinen R (1999) Subfield- and layer-specific changes in parvalbumin, calretinin and calbindin-D28K immunoreactivity in the entorhinal cortex in Alzheimer's disease. *Neuroscience* **92,** 515-532.

[15] Fonseca M, Soriano E (1995) Calretinin-immunoreactive neurons in the normal human temporal cortex and in Alzheimer's disease. *Brain Res* **691,** 83-91.

[16] Hof PR, Nimchinsky EA, Celio MR, Bouras C, Morrison JH (1993) Calretinin-immunoreactive neocortical interneurons are unaffected in Alzheimer's disease. *Neurosci Lett* **152,** 145-148.

[17] Sampson VL, Morrison JH, Vickers JC (1997) The cellular basis for the relative resistance of parvalbumin and calretinin immunoreactive neocortical neurons to the pathology of Alzheimer's disease. *Exp Neurol* **145,** 295-302.

[18] Cobb SR, Buhl EH, Halasy K, Paulsen O, Somogyi P (1995) Synchronization of neuronal activity in hippocampus by individual GABAergic interneurons. *Nature* **378,** 75-78.

[19] Gulyas AI, Hajos N, Freund TF (1996) Interneurons containing calretinin are specialized to control other interneurons in the rat hippocampus. *J Neurosci* **16,** 3397-3411.

[20] Schurmans S, Schiffmann SN, Gurden H, Lemaire M, Lipp HP, Schwam V, Pochet R, Imperato A, Bohme GA, Parmentier M (1997) Impaired long-term potentiation induction in dentate gyrus of calretinin-deficient mice. *Proc Natl Acad Sci U S A* **94,** 10415-10420.

[21] Blanchard V, Moussaoui S, Czech C, Touchet N, Bonici B, Planche M, Canton T, Jedidi I, Gohin M, Wirths O, Bayer TA, Langui D, Duyckaerts C, Tremp G, Pradier L (2003) Time sequence of maturation of dystrophic neurites associated with Abeta deposits in APP/PS1 transgenic mice. *Exp Neurol* **184,** 247-263.

[22] Caballero C, Jimenez S, Moreno-Gonzalez I, Baglietto-Vargas D, Sanchez-Varo R, Gavilan MP, Ramos B, Del Rio JC, Vizuete M, Gutierrez A, Ruano D, Vitorica J (2007) Interindividual variability in the expression of the mutated form of hPS1M146L determined the production of Abeta peptides in the PS1xAPP transgenic mice. *J Neurosci Res* **85,** 787-797.

[23] Jimenez S, Baglietto-Vargas D, Caballero C, Moreno-Gonzalez I, Torres M, Sanchez-Varo R, Ruano D, Vizuete M, Gutierrez A, Vitorica J (2008) Inflammatory response in the hippocampus of PS1M146L/APP751SL mouse model of Alzheimer's disease: age-dependent switch in the microglial phenotype from alternative to classic. *J Neurosci* **28,** 11650-11661.

[24] Franklin KBJ, Paxinos G (2008) *The mouse brain in stereotaxic coordinates*, Academic Press.

[25] Dorph-Petersen KA, Nyengaard JR, Gundersen HJ (2001) Tissue shrinkage and unbiased stereological estimation of particle number and size. *J Microsc* **204,** 232-246.

[26] Schmitz C, Hof PR (2005) Design-based stereology in neuroscience. *Neuroscience* **130,** 813-831.

[27] West MJ (1999) Stereological methods for estimating the total number of neurons and synapses: issues of precision and bias. *Trends Neurosci* **22,** 51-61.

[28] Gundersen HJ, Jensen EB, Kieu K, Nielsen J (1999) The efficiency of systematic sampling in stereology – reconsidered. *J Microsc* **193,** 199-211.

[29] Matyas F, Freund TF, Gulyas AI (2004) Immunocytochemically defined interneuron populations in the hippocampus of mouse strains used in transgenic technology. *Hippocampus* **14,** 460-481.

[30] Abraham H, Meyer G (2003) Reelin-expressing neurons in the postnatal and adult human hippocampal formation. *Hippocampus* **13,** 715-727.

[31] Jinno S, Kosaka T (2006) Cellular architecture of the mouse hippocampus: a quantitative aspect of chemically defined GABAergic neurons with stereology. *Neurosci Res* **56,** 229-245.

[32] Klausberger T, Somogyi P (2008) Neuronal diversity and temporal dynamics: the unity of hippocampal circuit operations. *Science* **321,** 53-57.

[33] Heizmann CW, Braun K (1992) Changes in Ca(2+)-binding proteins in human neurodegenerative disorders. *Trends Neurosci* **15,** 259-264.

[34] Iacopino AM, Christakos S (1990) Specific reduction of calcium-binding protein (28-kilodalton calbindin-D) gene expression in aging and neurodegenerative diseases. *Proc Natl Acad Sci U S A* **87,** 4078-4082.

[35] Palop JJ, Jones B, Kekonius L, Chin J, Yu GQ, Raber J, Masliah E, Mucke L (2003) Neuronal depletion of calcium-dependent proteins in the dentate gyrus is tightly linked to Alzheimer's disease-related cognitive deficits. *Proc Natl Acad Sci U S A* **100,** 9572-9577.

[36] Popovic M, Caballero-Bleda M, Kadish I, Van GT (2008) Subfield and layer-specific depletion in calbindin-D28K, calretinin and parvalbumin immunoreactivity in the dentate gyrus of amyloid precursor protein/presenilin 1 transgenic mice. *Neuroscience* **155,** 182-191.

[37] Mazurek MF, Beal MF (1991) Cholecystokinin and somatostatin in Alzheimer's disease postmortem cerebral cortex. *Neurology* **41,** 716-719.

[38] Liu Y, Yoo MJ, Savonenko A, Stirling W, Price DL, Borchelt DR, Mamounas L, Lyons WE, Blue ME, Lee MK (2008) Amyloid pathology is associated with progressive monoaminergic neurodegeneration in a transgenic mouse model of Alzheimer's disease. *J Neurosci* **28,** 13805-13814.

[39] Haass C, Selkoe DJ (2007) Soluble protein oligomers in neurodegeneration: lessons from the Alzheimer's amyloid beta-peptide. *Nat Rev Mol Cell Biol* **8,** 101-112.

[40] Suh YH, Checler F (2002) Amyloid precursor protein, presenilins, and alpha-synuclein: molecular pathogenesis and pharmacological applications in Alzheimer's disease. *Pharmacol Rev* **54,** 469-525.

[41] Walsh DM, Selkoe DJ (2007) A beta oligomers – a decade of discovery. *J Neurochem* **101,** 1172-1184.

[42] De Vos KJ, Grierson AJ, Ackerley S, Miller CC (2008) Role of axonal transport in neurodegenerative diseases. *Annu Rev Neurosci* **31,** 151-173.

[43] Smith KD, Kallhoff V, Zheng H, Pautler RG (2007) *In vivo* axonal transport rates decrease in a mouse model of Alzheimer's disease. *Neuroimage* **35,** 1401-1408.

[44] Stokin GB, Lillo C, Falzone TL, Brusch RG, Rockenstein E, Mount SL, Raman R, Davies P, Masliah E, Williams DS, Goldstein LS (2005) Axonopathy and transport deficits early

in the pathogenesis of Alzheimer's disease. *Science* **307,** 1282-1288.

[45] Zhu X, Moreira PI, Smith MA, Perry G (2005) Alzheimer's disease: an intracellular movement disorder? *Trends Mol Med* **11,** 391-393.

[46] Acsady L, Halasy K, Freund TF (1993) Calretinin is present in non-pyramidal cells of the rat hippocampus–III. Their inputs from the median raphe and medial septal nuclei. *Neuroscience* **52**, 829-841.